China Ocean Eng., 2019, Vol. 33, No. 6, P. 685–693
DOI: 10.1007/s13344-019-0066-9, ISSN 0890-5487
http://www.chinaoceanengin.cn/ E-mail: coe@nhri.cn

Upper Bound Solutions for Uplift Ultimate Bearing Capacity of Suction Caisson Foundation

DAI Guo-liang, ZHU Wen-bo*, ZHAI Qian, GONG Wei-ming, ZHAO Xue-liang

School of Civil Engineering, Southeast University, Nanjing 210096, China

Received July 10, 2018; revised June 4, 2019; accepted July 14, 2019

Abstract

Suction caisson foundation derives most of their uplift resistance from passive suction developed during the pullout movement. It was observed that the passive suction generated in soil at the bottom of the caisson and the failure mode of suction caisson foundation subjecting pullout loading behaves as a reverse compression failure mechanism. The upper bound theorems have been proved to be a powerful method to find the critical failure mechanism and critical load associated with foundations, buried caissons and other geotechnical structures. However, limited attempts have been reported to estimate the uplift bearing capacity of the suction caisson foundation using the upper bound solution. In this paper, both reverse failure mechanisms from Prandtl and Hill were adopted as the failure mechanisms for the computation of the uplift bearing capacity of the suction caisson. New equations were proposed based on both failure mechanisms to estimate the pullout capacity of the suction caisson. The proposed equations were verified by the test results and experimental data from published literature. And the two solutions agree reasonably well with the other test results. It can be proved that both failure mechanisms are reasonably and more consistent with the actual force condition.

Key words: suction caisson foundation, bearing capacity, upper bound solution, failure mechanism

Citation: Dai, G. L., Zhu, W. B., Zhai, Q., Gong, W. M., Zhao, X. L., 2019. Upper bound solutions for uplift ultimate bearing capacity of suction caisson foundation. China Ocean Eng., 33(6): 685–693, doi: 10.1007/s13344-019-0066-9

1 Introduction

Suction caissons have been widely used in as foundations in offshore oil and gas industry and have recently extended to offshore wind turbines. On the other hand, suction caisson foundations are also commonly adopted in the mooring systems. However, there are still no wide spread engineering specifications on design and calculation of uplift bearing capacity for the suction caisson foundation. Existing methods for estimating the pullout capacity of suction are mainly based on experiments or finite element analysis (Rao et al., 1997; Deng and Carter, 2002; Feng et al., 2016; Zhai and Li, 2017; Du et al., 2017). Andersen et al. (1993) carried out four field tests to study the pullout behavior of suction caissons in soft clay and concluded that the ultimate capacity may be calculated by assuming a reverse bearing capacity failure. They also suggested that an upper limit could be solved by assuming a failure mechanism which is similar to the approach to compute the bearing capacity of the shallow foundation as introduced by Terzaghi (1943). The upper bound theorem has been proved to be a powerful tool for the analysis of the plastic collapse associated with shallow foundations, buried caissons and circular foundations (Chen, 1975; Yang, 2002; Wang, 2008). However, limited attempts have been reported to estimate the pullout capacity of the suction caisson foundation using the upper bound solution.

In this paper, both reverse Prandtl failure mode and reverse Hill failure mode were adopted to represent the failure mechanism of suction caisson subjected to pullout loading. An upper bound method for calculating uplift bearing capacity of suction caisson foundation was based on these two failure modes. The proposed equations were verified by the test results and the experimental data from published literature. It shows that the results from proposed equations agree well with the experimental results. Subsequently, parametric studies were also carried out to investigate the effect of soil weight, friction angle, cohesion and friction coefficient on the pullout capacity of suction caisson.

2 Literature review

Various studies on the pullout resistance of suction caisson from different researchers (Bang et al., 2011; Deng and

Foundation item: This paper was financially supported by the National Key Research and Development Program (Grant No. 2017YFC0703408), the National Natural Science Foundation of China (Grant Nos. 51678145 and 51878160).

*Corresponding author. E-mail: 763566305@qq.com

Carter, 2002; Gao et al., 2013; Singh et al., 1996; El-Gharbawy and Olson, 1998; Hogervorst, 1980; Watson and Randolph, 1997) have been reported in recent years. The uplift bearing capacity of the suction caisson with respect to different types of soil, different loading rates and different aspect ratios had been investigated in these studies. It was observed that the passive suction generated in the soil at the bottom of the caisson and failure occurs as a reverse failure mechanism. The reverse failure mechanism is widely used for the estimation of the uplift bearing capacity of suction caissons loaded under partial conditions and undrained conditions (Du et al., 2015; Mana et al., 2014; Guo et al., 2014; Feng et al., 2016; Zhai and Li, 2017). In other words, the works from previous researchers have suggested that pullout failure of the suction caisson foundation under undrained condition could be considered similar to the reverse failure mechanism. However, the bottom resistance of the suction caisson has not been properly understood and quantified. The upper bound theorems are commonly used for the analysis of the plastic collapse associated with shallow foundations, buried caissons and circular foundations (Chen, 1975; Yang, 2002; Chen, 2008; Zhang and Fu, 2010; Cheng et al., 2014; Liu et al., 2015). Wang (2008) adopted the concept of "reverse bearing capacity" and deduced the upper bound solution for ultimate bearing capacity of suction caisson foundation based on Prandtl failure mechanism (Fig. 1). It is known that Prandtl failure mode was proposed based on the assumption that the foundation is subjected to a compression load. However, the suction caisson is subjected to pullout loading and Prandtl failure mode may not be applicable any more. After that, very few attempts have been made to study the upper bound solution on the uplift bearing capacity of suction caisson foundations. In order to predict the uplift bearing capacity of suction caisson foundation under undrained conditions, two failure mechanisms including reverse Prandtl mechanism and reverse Hill mechanism were assumed in this paper.

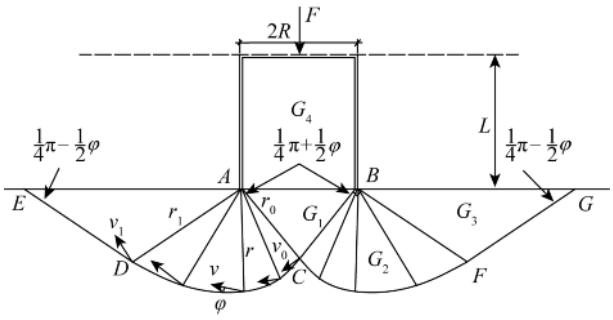

Fig. 1. Prandtl failure mechanism.

3 Two reverse failure mechanisms

Two distinct failure mechanisms, referred to as M1 and M2, are utilized in the analysis. M1 is the reverse Prandtl failure mechanism and M2 is the Hill reverse failure mode. The Prandtl reverse failure mechanism means that the active wedge under the caisson becomes the passive wedge at the vertical pullout loads, at the same time, the direction of the principal stress is horizontal and the minor principal stress is vertical. The angle between the direction of horizontal plane and the failure surface is $45°-\varphi/2$, so it is different from Prandtl failure mechanism (the angle is $45°+\varphi/2$), and the logarithmic spiral direction is opposite. The upper bound theorems, which assumes a perfectly plastic soil model with an associated flow rule, states that the internal power dissipated by any kinematically admissible velocity field can be equated to the power dissipated by the external loads and so enables a strict upper bound on the true limit load to be deduced.

3.1 Reverse Prandtl failure mechanism

The configuration of the suction caisson foundation here was described through two parameters-the radius R, the caisson buried depth L. An overall schematic illustration of M1 is shown in Fig. 2, and the kinematic mechanism and the associated velocity field are shown in Fig. 3. Since the movement is symmetrical about the footing, it is only necessary to consider the movement on the left-side of M1. The

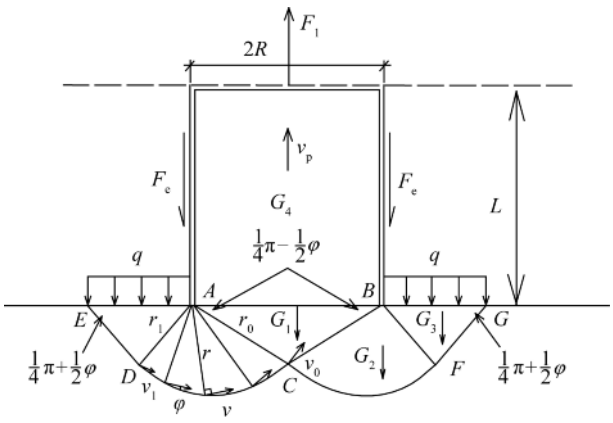

Fig. 2. Reverse Prandtl failure mechanism.

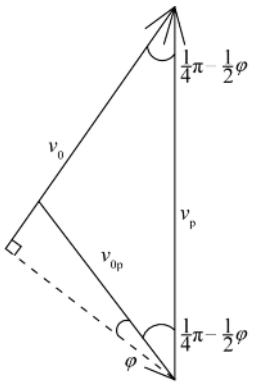

Fig. 3. Velocity hodographs.

wedge *ABC*, with the weight G_1, moves with velocity v_0 but makes an angle φ, the friction angle of soil with the linear failure surface *AC*. The logarithmic spiral *ACD* with the weight G_2, moves with velocity v but makes an angle φ, with the curved failure surface *CD*. The wedge *ADE* with the weight G_3, moves with velocity v_1. The suction caisson foundation moves vertically with velocity v_p. Soil may slide either along the foundation surface, referred to as interface shear with limiting shear stress $a \cdot c$. At the same time, the soil weight above the bottom of the caisson was considered in the upper bound solution of M1. And the soil weight above the bottom of the caisson is equivalent to q.

From the velocity profile shown in Fig. 3, it is possible to deduce the velocity at the failure surfaces of *AC*, *CD* and *ED*.

(1) Failure surface *AC*

$$v_0 = \frac{1}{2} v_p \sec\left(\frac{\pi}{4} - \frac{\varphi}{2}\right), \tag{1}$$

where v_p is the virtual velocity in the direction of pullout and φ is the friction angle.

(2) Failure surface *CD*

$$v = v_0 e^{-\theta \tan\varphi} = \frac{1}{2} v_p \sec\left(\frac{\pi}{4} - \frac{\varphi}{2}\right) e^{-\theta \tan\varphi}, \tag{2}$$

where θ is the angle between v and v_0.

(3) Failure surface *DE*

$$v_1 = v_0 e^{-\frac{\pi}{2}\tan\varphi} = \frac{1}{2} v_p \sec\left(\frac{\pi}{4} - \frac{\varphi}{2}\right) e^{-\frac{\pi}{2}\tan\varphi}. \tag{3}$$

Through the geometric relationship obtained can be the size of failure surface

$$r = r_0 e^{-\theta \tan\varphi} = R \sec\left(\frac{\pi}{4} - \frac{\varphi}{2}\right) e^{-\theta \tan\varphi}; \tag{4}$$

$$r_1 = r_0 e^{-\frac{\pi}{2}\tan\varphi} = R \sec\left(\frac{\pi}{4} - \frac{\varphi}{2}\right) e^{-\frac{\pi}{2}\tan\varphi}; \tag{5}$$

$$AE = 2r_1 \cos\left(\frac{\pi}{4} + \frac{\varphi}{2}\right) = 2R \tan\left(\frac{\pi}{4} - \frac{\varphi}{2}\right) e^{-\frac{\pi}{2}\tan\varphi}. \tag{6}$$

By considering the mechanism M1, the work dissipation is calculated for each zone. It is assumed that the energy dissipation rate in the surface area express as vc.

1. Wedge zone *ABC*

As shown in Fig. 1, incremental internal work due to the conic section *ABC*

$$W_1 = (v_0 \cos\varphi) c S_{\overline{ABC}} = \frac{1}{2} v_p \pi R^2 c \cos\varphi \sec^2\left(\frac{\pi}{4} - \frac{\varphi}{2}\right), \tag{7}$$

where c is the cohesion.

The energy dissipation work of *ABC* due to self-weight

$$W_{G_1} = -\frac{1}{3} \gamma \pi R^3 v_p \tan\left(\frac{\pi}{4} - \frac{\varphi}{2}\right), \tag{8}$$

where γ is the weight of soil.

2. Logarithmic spiral zone *ACD*

Incremental internal work due to the logarithmic spiral *DCF*

$$W_2 = \int_0^{\frac{\pi}{2}} 2\pi c v \cos\varphi \left[R - r\cos\left(\frac{\pi}{4} - \frac{\varphi}{2} + \theta\right)\right] \frac{r}{\cos\varphi} \mathrm{d}\theta = v_p c \pi R^2 \sec^2\left(\frac{\pi}{4} - \frac{\varphi}{2}\right) \left[\frac{1 - e^{-\pi\tan\varphi}}{2\tan\varphi} - f_1 + \tan\left(\frac{\pi}{4} - \frac{\varphi}{2}\right) f_2\right], \tag{9}$$

where f_1 and f_2 are reported in Appendix B.

Incremental internal work due to the logarithmic spiral deformation *ACD*

$$W_4 = \int_0^{\frac{\pi}{2}} \int_0^r 2\pi c v \cos\varphi \left[R - \bar{r}\cos\left(\frac{\pi}{4} - \frac{\varphi}{2} + \theta\right)\right] \frac{\mathrm{d}\bar{r}}{\cos\varphi} \mathrm{d}\theta = v_p c \pi R^2 \sec^2\left(\frac{\pi}{4} - \frac{\varphi}{2}\right) \left[\frac{1 - e^{-\pi\tan\varphi}}{2\tan\varphi} - \frac{1}{2} f_1 + \frac{1}{2}\tan\left(\frac{\pi}{4} - \frac{\varphi}{2}\right) f_2\right]. \tag{10}$$

The energy dissipation work of *ACD* due to self-weight

$$W_{G_2} = -\gamma \int_0^{\frac{\pi}{2}} \int_0^r 2\pi v_v \left[R - \bar{r}\cos\left(\frac{\pi}{4} - \frac{\varphi}{2} + \theta\right)\right] \bar{r} \mathrm{d}\bar{r} \mathrm{d}\theta = \frac{1}{2} \gamma v_p \pi R^3 \sec^2\left(\frac{\pi}{4} - \frac{\varphi}{2}\right) \left\{-f_1 + \tan\left(\frac{\pi}{4} - \frac{\varphi}{2}\right) f_2 + \frac{1}{3}\sec^2\left(\frac{\pi}{4} - \frac{\varphi}{2}\right) \left[\frac{1 - e^{-2\pi\tan\varphi}}{4\tan\varphi} + \cos 2\left(\frac{\pi}{4} - \frac{\varphi}{2}\right) f_3 - \sin 2\left(\frac{\pi}{4} - \frac{\varphi}{2}\right) f_4\right]\right\}, \tag{11}$$

where f_3 and f_4 are reported in Appendix B.

3. Wedge zone *ADE*

Incremental internal work due to the wedge *ADE*

$$W_3 = (v_1 \cos\varphi) c S_{\overline{EDFG}} = \frac{1}{2} v_p c \pi R^2 \cos\varphi \sec^2\left(\frac{\pi}{4} - \frac{\varphi}{2}\right) e^{-\pi\tan\varphi} \left[3\tan\left(\frac{\pi}{4} - \frac{\varphi}{2}\right) e^{-\frac{\pi}{2}\tan\varphi} + 2\right]. \tag{12}$$

The energy dissipation work of *ADE* due to self-weight

$$W_{G_3} = \frac{2}{3} \gamma \pi R^3 v_p \tan^2\left(\frac{\pi}{4} - \frac{\varphi}{2}\right) e^{-\frac{3}{2}\pi\tan\varphi} \left[\tan\left(\frac{\pi}{4} - \frac{\varphi}{2}\right) e^{-\frac{\pi}{2}\tan\varphi} + 1\right]. \tag{13}$$

4. Energy dissipation work on the interface of the caisson outer wall and the soil

$$W_5 = 2\pi R L a c v_p, \tag{14}$$

where a is the coefficient of friction between the caisson and the soil and L is the Caisson buried depth.

5. Energy dissipation rate of soil gravity in suction caisson

$$W_{G_4} = -\gamma v_p \pi R^2 L. \tag{15}$$

6. Incremental external work due to the surcharge loading

$$W_q = 2 v_p \pi R^2 \tan^2\left(\frac{\pi}{4} - \frac{\varphi}{2}\right) e^{-\pi\tan\varphi} \left[\tan\left(\frac{\pi}{4} - \frac{\varphi}{2}\right) e^{-\frac{\pi}{2}\tan\varphi} + 1\right] q, \tag{16}$$

where q is the soil weight above the bottom of caisson.

7. Incremental external work due to the uplift load

$$W_{F_1} = v_p F_1. \tag{17}$$

8. Formulation of upper bound solution

With the balance of external work and internal work, Eq. (18) can be obtained as follows:

$$W_{F_1}+W_q+W_{G_1}+W_{G_2}+W_{G_3}+W_{G_4}=W_1+W_2+W_3+W_4+W_5. \tag{18}$$

Eq. (18) provides a general form of the upper bound solution for the reverse Prandtl failure mechanism. By substituting Eqs. (7)−(16) into Eq. (18), the ultimate pullout capacity of suction caisson can be obtained from Eq. (19) as follows:

$$\begin{aligned}F_1=&-2f_6\mathrm{e}^{-\pi\tan\varphi}(f_7+1)q+\frac{1}{3}\gamma\pi R^3\tan\left(\frac{\pi}{4}-\frac{\varphi}{2}\right)-\\&\frac{1}{2}\gamma Rf_5\left\{-f_1+\tan\left(\frac{\pi}{4}-\frac{\varphi}{2}\right)f_2+\frac{1}{3}\sec^2\left(\frac{\pi}{4}-\frac{\varphi}{2}\right)\right.\\&\left.\left[\frac{1-\mathrm{e}^{-2\pi\tan\varphi}}{4\tan\varphi}+\cos 2\left(\frac{\pi}{4}-\frac{\varphi}{2}\right)f_3-\sin 2\left(\frac{\pi}{4}-\frac{\varphi}{2}\right)f_4\right]\right\}-\\&\frac{2}{3}\gamma Rf_6\mathrm{e}^{-\frac{3}{2}\pi\tan\varphi}(f_7+1)+\gamma\pi R^2L+\frac{1}{2}c\cos\varphi f_5+\\&cf_5\left[\frac{1-\mathrm{e}^{-\pi\tan\varphi}}{2\tan\varphi}-f_1+\tan\left(\frac{\pi}{4}-\frac{\varphi}{2}\right)f_2\right]+\\&\frac{1}{2}c\cos\varphi f_5\mathrm{e}^{-\pi\tan\varphi}(3f_7+2)+\\&cf_5\left[\frac{1-\mathrm{e}^{-\pi\tan\varphi}}{2\tan\varphi}-\frac{1}{2}f_1+\frac{1}{2}\tan\left(\frac{\pi}{4}-\frac{\varphi}{2}\right)f_2\right]+2\pi RLac.\end{aligned} \tag{19}$$

3.2 Reverse Hill failure mechanism

An overall schematic illustration of the problem, the kinematic mechanism and the associated velocity field is shown in Fig. 4. Since the movement is symmetrical about the footing, it is only necessary to consider the movement on the left-side of M2. The wedge *OAC*, with weight G1, moves with velocities v_0 but makes the angle φ, the friction angle of soil, with the linear failure surface *OC*. The Logarithmic spiral *AFC*, with weight G2, moves with velocity v but makes the angle φ, with the curved failure surface *CF*. The wedge *AEF*, with weight G3, move with velocity v_1. The suction caisson moves vertically with velocity v_p. Soil may slide either along the foundation surface, referred to as interface shear with limiting shear stress ac. And the soil weight above the bottom of caisson is equivalent to q.

The upper bound solution of M2 is

$$\begin{aligned}F_2=&-f_6\mathrm{e}^{-\pi\tan\varphi}(f_7+2)q+\frac{1}{6}\gamma\pi R^3\tan\left(\frac{\pi}{4}-\frac{\varphi}{2}\right)-\\&\frac{1}{8}\gamma Rf_5\left\{-f_1+\tan\left(\frac{\pi}{4}-\frac{\varphi}{2}\right)f_2+\frac{1}{3}\sec^2\left(\frac{\pi}{4}-\frac{\varphi}{2}\right)\right.\\&\left.\left[\frac{1-\mathrm{e}^{-2\pi\tan\varphi}}{4\tan\varphi}+\cos 2\left(\frac{\pi}{4}-\frac{\varphi}{2}\right)f_3-\sin 2\left(\frac{\pi}{4}-\frac{\varphi}{2}\right)f_4\right]\right\}-\\&\frac{1}{6}\gamma Rf_6\mathrm{e}^{-\frac{3}{2}\pi\tan\varphi}(f_7+2)+\gamma\pi R^2L+\frac{1}{4}c\cos\varphi f_5+\\&\frac{1}{2}cf_5\left[\frac{1-\mathrm{e}^{-\pi\tan\varphi}}{2\tan\varphi}-f_1+\tan\left(\frac{\pi}{4}-\frac{\varphi}{2}\right)f_2\right]+\\&\frac{1}{4}c\cos\varphi f_5\mathrm{e}^{-\pi\tan\varphi}(3f_7+2)+\\&\frac{1}{2}cf_5\left[\frac{1-\mathrm{e}^{-\pi\tan\varphi}}{2\tan\varphi}-\frac{1}{2}f_1+\frac{1}{2}\tan\left(\frac{\pi}{4}-\frac{\varphi}{2}\right)f_2\right]+2\pi RLac,\end{aligned} \tag{20}$$

where f_5, f_6 and f_7 are reported in Appendix B.

4 Model test

In order to prove the above theory, several model tests were carried out for study. The tests were conducted in a steel tank with dimensions of 1 m×1 m×1.2 m (Fig. 5). A servo actuator was used to provide the monotonic or the sustained pullout loads. The pullout load and the corresponding upward displacement were measured by a load cell and an LVDT, respectively. The MC #4 suction caisson model, made of perspex and MC #1−#3 suction caisson models, made of steel and the corresponding dimensions are given in Fig. 6. The soil used in the model tests was soft clay. The soil sample is prepared by mud sedimentation. The prepared soil sample parameters are shown in Table 1. In all model tests, pullout loading was applied after allowing the soil to remain undisturbed for 7 days.

Deng and Carter (2002) and Singh et al. (1996) suggested that the pullout rate is 16 mm/min when soil is under

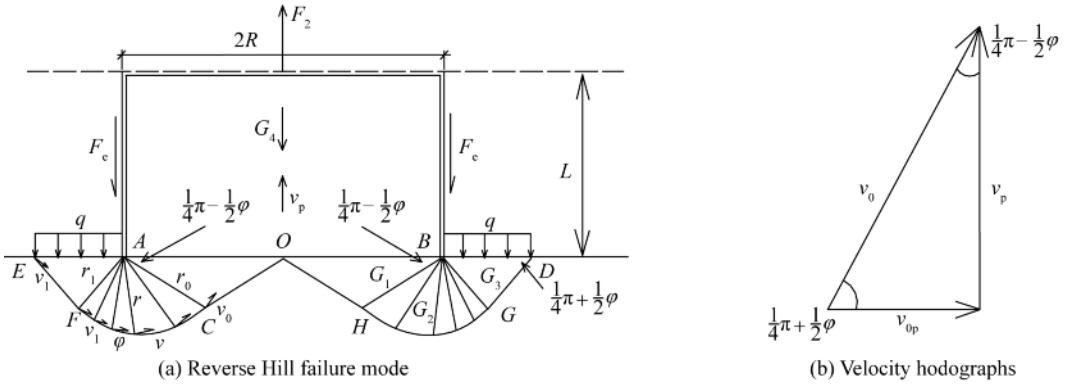

Fig. 4. Reverse Hill failure mechanism M2.

Fig. 5. Suction caisson model test.

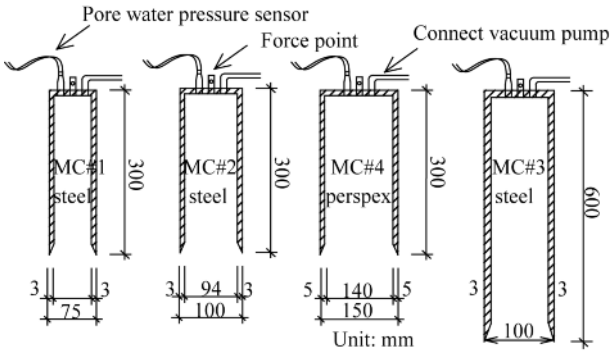

Fig. 6. Suction caisson model.

Table 1 Parameters of soil sample

W (%)	γ (kN/m^3)	LL (%)	PL (%)	I_P	Su
38.6	17.6	46.6	28.8	17.8	9.3

the undrained condition. As the size of the caisson models is close to the caisson models in the literature, the uplift rate of this test adopts the same pullout rate. Fig. 7 shows the pullout load-displacement behavior of model caissons. The ultimate bearing capacities of MC #1−#4 caisson models are 120.8 N, 186.0 N, 345.6 N and 287.3 N, respectively.

The results of test and the upper bound solutions are listed in Table 2. It can be seen from Table 2 that F_1 solutions agree reasonably well with the test results with differences in the range from 9.3% to 13.1%, and F_2 solutions with differences in the range from 1.8% to 7.8%. The two upper bound solutions used in this paper are smaller than those of F_3 of completely Prandtl failure mechanism of Wang (2008) and closer to the test results.

5 Comparison with experimental values

Singh et al. (1996), Shi et al. (2003), Jiao et al. (2006), El-Gharbawy and Olson (1998) and Chen et al. (2012) have performed the vertical uplift tests for suction caisson foundations under the undrained condition. The results of these tests and the upper bound solutions for the ultimate uplift load are shown in Fig. 8. The meaning of the 1:1 line is that the test values are equal to the calculated values. The points in Fig. 5 are the upper bound solutions, if the point is close to the line, it can be known that the upper bound solutions agree well with the test results. The two upper bound solutions used in this paper are smaller than those of complete Prandtl failure mechanism of Wang (2008) and closer to the test results. The comparisons presented that the upper bound solutions can be applied to suction caissons for estimating the uplift ultimate bearing capacity under the undrained condition.

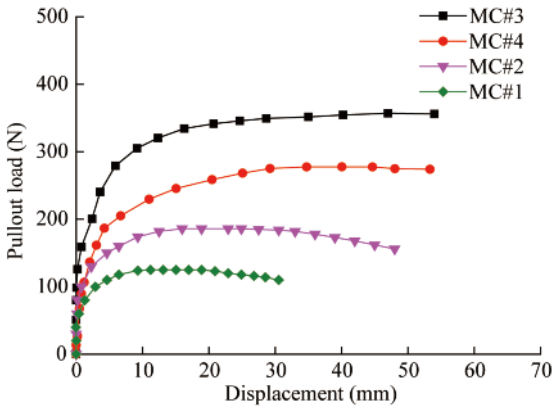

Fig. 7. Pullout load-displacement behavior of caissons.

6 Parameters study for upper bound solution

Because the law of M1 is similar to M2, parameters study was performed to the upper bound solution of M1, with basic configuration dimensions γ=20 kN/m^3, R=3 m, L=10 m, a=1, unless otherwise stated. The bearing capacity is compared in the case of c (=10 kPa, 20 kPa, 30 kPa) for different values of φ in Fig. 9. In comparison, the value of c is larger and the value of bearing capacity is higher. The bearing capacity is compared in the case of φ (=10°, 20°, 30°) for different values of c in Fig. 10. In comparison, the value of c is larger and the value of the bearing capacity is higher. The bearing capacity is compared in the case of φ (=10°, 20°, 30°) for different values of q in Fig. 11. In comparison, the value of q is higher and the value of the bearing capacity is smaller in the present analysis.

Table 2 Analysis of calculated and experimental results

No.	D (mm)	L/D	Su (kPa)	Test (N)	F_1 (N)	Diff.1 (%)	F_2 (N)	Diff.2 (%)	F_3 (N)	Diff.3 (%)
1	75	4.0	9.3	120.8	134.3	11.2	125.4	3.8	156.7	29.7
2	100	3.0	9.3	186.0	210.3	13.1	199.8	7.4	264.5	42.2
3	100	6.0	9.3	345.6	378.9	9.6	352.1	1.8	413.2	19.5
4	150	2.0	9.3	287.3	314.3	9.3	296.7	3.2	342.1	19.1

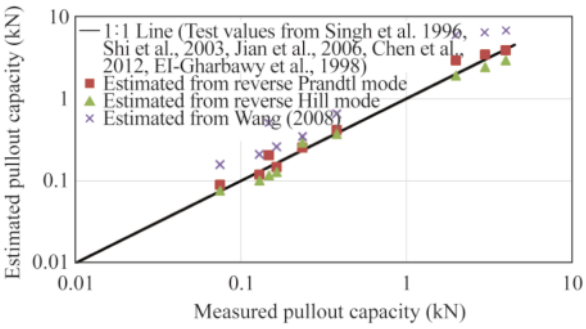

Fig. 8. Verification of upper bound solutions.

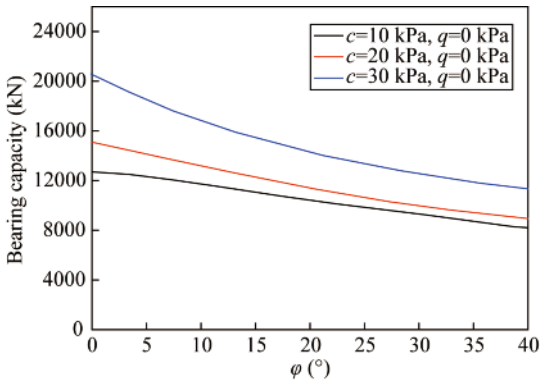

Fig. 9. Curve of upper bound solution and φ.

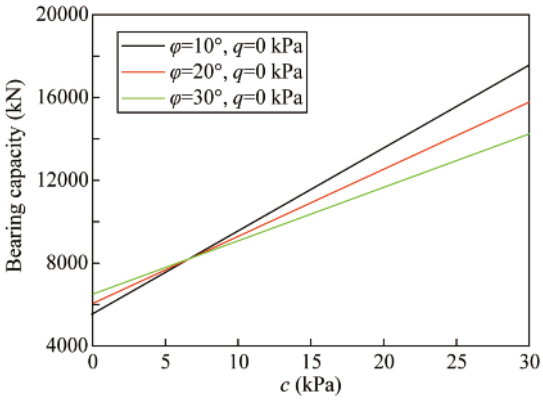

Fig. 10. Curve of upper bound solution and c.

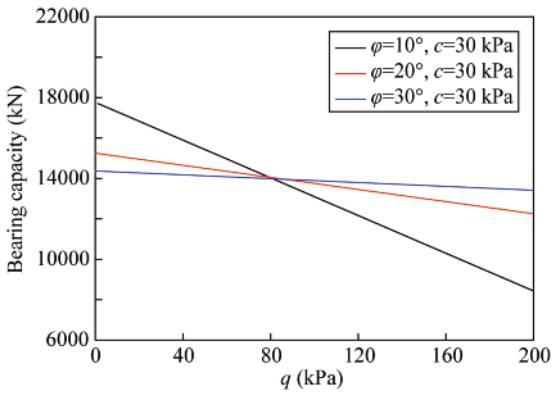

Fig. 11. Curve of upper bound solution and q in comparison with M1 and M2.

From Fig. 2 and Fig. 4, it can be observed that both reverse Prandtl failure mechanism and reverse Hill failure mechanism have the same initial speed v_p. The speed v of M1 is twice that of M2, but r of M1 is half that of M2. The primary influencing factor of both upper bound solutions between M1 and M2 is the caisson radius. In order to analyze the radius of caisson on the upper bound solution of the two mechanisms, the depth of the caisson is 10 m, and other parameters, γ=20 kN/m^3, a=1.

Fig. 12 shows the respective results of M1 and M2 mechanisms with c=10 kPa, 20 kPa and 30 kPa, considering an interface friction coefficient a=1 and other fixed parameters. It can be observed that the upper bound solutions can be improved by increasing the radius of caisson. The upper bound solution of M2 is smaller than that of M1 for the same aspect ratio. When the radius gradually increases, the results of the two upper bound solutions deviate greatly.

7 Bottom resistance of the suction caisson

In order to quantify the bottom resistance of the suction caisson under undrained conditions, Table 3 provides a comparison of M1 and M2 results. F_1 is the upper bound solution of M1, F_2 is the upper bound solution of M2, N_1 is the bottom resistance of caissons provided by M1, N_2 is the bottom resistance of caissons provided by M2. For the N part, the bearing capacity of N_1 accounts for 6%−23% of the upper limit solution of M1 and the bearing capacity of N_2 accounts for 4%−13% of the upper limit solution of M2. It may be noted that the bearing capacities of N_1 are slightly higher than those of N_2.

8 Effect of interface roughness factor for M1

The failure mechanism was found to be affected by the foundation-soil interface roughness factor a. In Fig. 13, a=0 indicates that the interface between caisson and soil is fully-smooth, and a=1 indicates that the interface between caisson and soil is fully-rough. Also for an intermediate roughness coefficient of a=0.6, M1 is used in the following calculations. The depth of the caisson is 10 m, the radius is 3 m, and the soil weight is 20 kN/m^3. It can be seen that the fully-smooth upper bound solution of the interface between caisson and soil is less than the fully-rough upper bound solution, and when c is higher, the value of upper bound solution is higher. But when q is higher, the value of upper bound solution is smaller.

9 Conclusions

This paper has presented two failure mechanisms for analyzing the uplift bearing capacity of suction caisson foundation using the upper bound method of the limit analysis theory. One is the reverse Prandtl failure mechanism and the other is the reverse Hill failure mechanism. The analysis of upper bound solutions and the comparison results

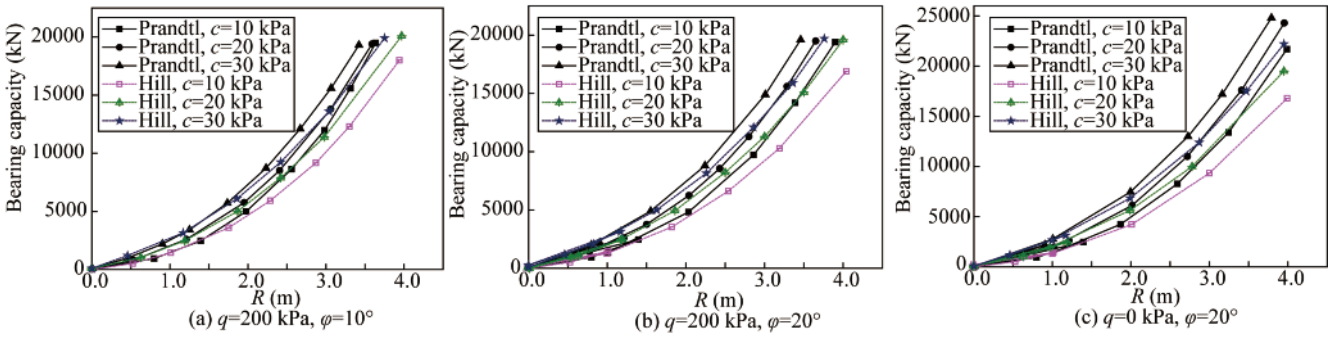

Fig. 12. Curve of upper bound solution and *R*.

Table 3 Bottom resistances of M1 and M2

No.	q (kPa)	c (kPa)	φ (°)	F_1 (×10³ kN)	N_1 (×10³ kN)	N_1/F_1	F_2 (×10³ kN)	N_2 (×10³ kN)	N_2/F_2
1	0	10	10	9.23	1.29	0.14	8.44	0.91	0.10
2	0	10	20	8.90	0.84	0.09	8.22	0.50	0.06
3	0	10	30	8.40	0.54	0.06	8.76	0.31	0.04
4	0	10	20	8.90	0.84	0.09	8.22	0.50	0.06
5	0	20	20	11.9	1.58	0.13	10.6	1.00	0.09
6	0	30	20	14.8	2.36	0.16	13.0	1.52	0.11
7	0	30	20	14.8	2.36	0.16	13.0	1.52	0.11
8	100	30	20	13.4	2.36	0.18	11.8	1.52	0.13
9	200	30	20	11.9	2.69	0.23	11.7	1.52	0.13

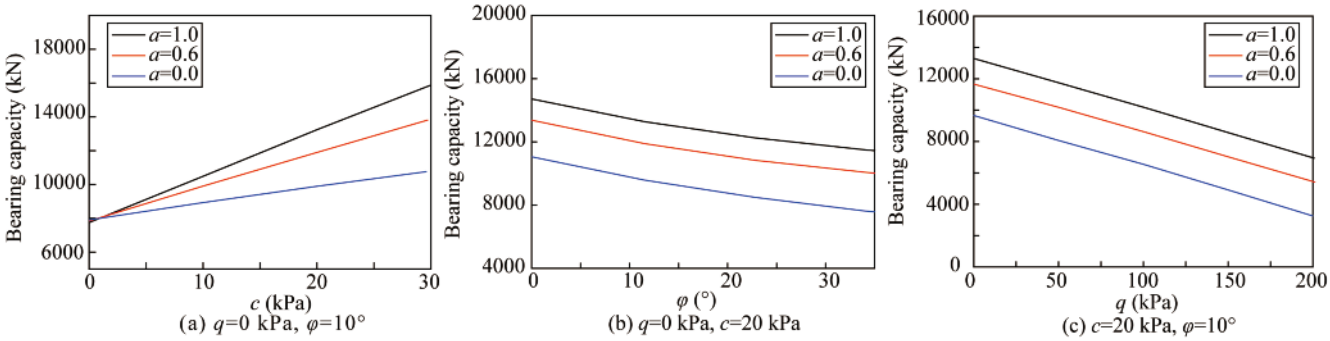

Fig. 13. Influence of the friction coefficient on the upper limit solution.

presented lead to the following conclusions.

(1) The F1 solutions agree reasonably well with the test results with differences in the range from 9.3% to 13.1%, and the F2 solutions with differences in the range from 1.8% to 7.8%. The two upper bound solutions used in this paper are smaller than those of F3 of completely Prandtl failure mechanism of Wang (2008) and closer to the test results. And the two solutions agree reasonably well with the other test results. It can be proved that both failure mechanisms are reasonably and more consistent with the actual force condition.

(2) The most critical bearing capacity factors are q, c, a. It can be observed that the upper bound solution of M1 can be improved by increasing the value of c, a, but reduced with q increasing.

(3) From the comparison results of the two mechanisms, both M1 and M2 mechanisms give the exact solution of bottom resistance of the suction caisson. It may be noted that the bearing capacity of N_1 accounts for 6%−23% of the upper limit solution of M1 and the bearing capacity of N_2 accounts for 4%−13% of the upper limit solution of M2. It can be seen that the bearing capacities of N_1 are slightly higher than the bearing capacities of N_2.

References

Andersen, K.H., Dyvik, R., Schrøder, K., Hansteen, O.E. and Bysveen, S., 1993. Field tests of anchors in Clay II: Predictions and interpretation, *Journal of Geotechnical Engineering*, 119(10), 1532–1549.

Bang, S., Jones, K.D., Kim, K.O., Kim, Y.S. and Cho, Y., 2011. Inclined loading capacity of suction piles in sand, *Ocean Engineering*, 38(7), 915–924.

Chen, H.F., 1975, *Limit Analysis and Soil Plasticity*, Elsevier Scientific Publishing Company, Amsterdam.

Chen, R., Gaudin, C. and Cassidy, M.J., 2012. Investigation of the vertical uplift capacity of deep water mudmats in clay, *Canadian Geo-*

technical Journal, 49(7), 853–865.

Chen, Z.L., 2008. *Upper Bound Limit Analysis of Circular Foundation Foundations Based on Non-Linear Damage Criterion*, MSc. Thesis, Central South University, Changsha. (in Chinese)

Cheng, F., Lian, J.J. and Wang, H.J., 2014. Upper-bound limit analysis of the vertical bearing capacity of circular shallow foundations, *Journal of Hunan University* (*Natural Sciences*), 41(6), 92–98. (in Chinese)

Deng, W. and Carter, J.P., 2002. A theoretical study of the vertical uplift capacity of suction caissons, *International Society of Offshore and Polar Engineers*, 12(2), 89–97.

Du, J.Q., Du, S.J., Shen, S.L. and Yin, Z.Y., 2015. Numerical investigation of the undrained compression and pull-out capacity of suction foundations in clay, *Polish Maritime Research*, 22(S1), 126–135.

Du, J.Q., Du, S.J., Shen, S.L. and Ma, X.F., 2017. Centrifuge evaluation of the influential factors in the uplift capacity of suction foundations in clay, *Marine Georesources & Geotechnology*, 35(4), 456–465.

El-Gharbawy, S. and Olson, R., 1998. The pullout capacity of suction caisson foundations for tension leg platforms, *Proceedings of the 8th International Offshore and Polar Engineering*, ISOPE, Montréal, pp. 531–536.

Feng, X., Pi, X.J., Feng, S.L. and Bian, C., 2016. Research on the uplift bearing capacity of suction caisson foundation under local tensile failure, *Procedia Engineering*, 166, 61–68.

Gao, Y.F., Qiu, Y., Li, B., Li, D.Y., Sha, C.M. and Zheng, X., 2013. Experimental studies on the anti-uplift behavior of the suction caissons in sand, *Applied Ocean Research*, 43, 37–45.

Guo, Z., Wang, L.Z. and Yuan, F., 2014. Set-up and pullout mechanism of suction caisson in a soft clay seabed, *Marine Georesources & Geotechnology*, 32(2), 135–154.

Hogervorst, J.R., 1980. Field trails with large diameter suction piles, *Proceedings of the 12th Annual Offshore Technology Conference OTC 3817*, OTC, Houston, pp. 217–222.

Jiao, B.T., Lu, X.B., Zhao, J. and Shi, Z.M., 2006. On the pullout bearing capacity of bucket foundation, *China Offshore Platform*, 21(3), 27–30. (in Chinese)

Liu, S.Q., Lu, K.L., Zhu, D.Y. and Jiang, Z.F., 2015. Calculation of ultimate bearing capacity of circular footing, *Journal of Engineering Geology*, 23(5), 1005–1012. (in Chinese)

Mana, D.S.K., Gourvenec, S. and Randolph, M.F., 2014. Numerical modelling of seepage beneath skirted foundations subjected to vertical uplift, *Computers and Geotechnics*, 55, 150–157.

Rao, S.N., Ravi, R. and Prasad, B.S., 1997. Pullout behavior of suction anchors in soft marine clays, *Marine Georesources & Geotechnology*, 15(2), 95–114.

Shi, X.C., Gong, X.N., Yu, J.L. and Chen, G.X., 2003. Experimental study on pull-out bearing capacity of bucket foundation, *Building Structure*, 33(8), 49–51, 56. (in Chinese)

Singh, B., Datta, M. and Gulhati, S.K., 1996. Pullout behavior of superpile anchors in soft clay under static loading, *Marine Georesources & Geotechnology*, 14(3), 217–236.

Terzaghi, K., 1943. *Theoretical Soil Mechanics*, John Wiley and Sons Inc., New York.

Wang, Z.Y., 2008. *A Study on Uplift Bearing Characteristics of Suction Caisson Foundation in Soft Ground*, Ph. D. Thesis, Dalian University of Technology, Dalian. (in Chinese)

Watson, P.G. and Randolph, M.F., 1997. Vertical capacity of caisson foundations in calcareous sediments, *Proceedings of the 7th International Offshore and Polar Engineering*, ISOPE, Honolulu, Hawaii, pp. 152–159.

Yang, X.L., 2002. *Limit Analysis Method and Its Application to Geotechnical Engineering with Linear and Nonlinear Failure Criteria*, Ph. D. Thesis, Central South University, Changsha. (in Chinese)

Zhai, H.B. and Li, D.Y., 2017. Experimental studies on modified suction caissons in fine sand subject to uplift loading, *Transactions of Tianjin University*, 23(6), 562–569.

Zhang, G.X. and Fu, J.S., 2010. Upper bound solution for bearing capacity of circular shallow foundation based on limit analysis, *Rock and Soil Mechanics*, 31(12), 3849–3854. (in Chinese)

Appendix A

In this appendix, we present different expressions for the incremental external work of mechanism M2, together with the internal energy dissipation for the same mechanism. From the velocity profile shown in Fig. 4b, it is possible to deduce the velocity at the failure surfaces *OC*, *CF* and *EF*.

Failure surface *OC*

$$v_0 = v_\mathrm{p}\sec\left(\frac{\pi}{4}-\frac{\varphi}{2}\right) \tag{A1}$$

Failure surface *CF*

$$v = v_0 \mathrm{e}^{-\theta\tan\varphi} = v_\mathrm{p}\sec\left(\frac{\pi}{4}-\frac{\varphi}{2}\right)\mathrm{e}^{-\theta\tan\varphi} \tag{A2}$$

Failure surface *EF*

$$v_1 = v_0 \mathrm{e}^{-\frac{\pi}{2}\tan\varphi} = v_\mathrm{p}\sec\left(\frac{\pi}{4}-\frac{\varphi}{2}\right)\mathrm{e}^{-\frac{\pi}{2}\tan\varphi}. \tag{A3}$$

Through the geometric relationship obtained can be the size of M2

$$r = r_0 \mathrm{e}^{-\theta\tan\varphi} = \frac{R}{2}\sec\left(\frac{\pi}{4}-\frac{\varphi}{2}\right)\mathrm{e}^{-\theta\tan\varphi}; \tag{A4}$$

$$r_1 = r_0 \mathrm{e}^{-\frac{\pi}{2}\tan\varphi} = \frac{R}{2}\sec\left(\frac{\pi}{4}-\frac{\varphi}{2}\right)\mathrm{e}^{-\frac{\pi}{2}\tan\varphi}; \tag{A5}$$

$$AE = 2r_1\cos\left(\frac{\pi}{4}+\frac{\varphi}{2}\right) = R\tan\left(\frac{\pi}{4}-\frac{\varphi}{2}\right)\mathrm{e}^{-\frac{\pi}{2}\tan\varphi}. \tag{A6}$$

Example derivations of plastic work

The work dissipation within the $c-\varphi$ soil considered in the paper can be expressed as follows:

Wedge zone *AOC*

As shown in Fig. 1, incremental internal work due to section *COH*

$$W_1 = (v_0\cos\varphi)cS_{\overline{COH}} = \frac{1}{4}v_\mathrm{p}\pi R^2 c\cos\varphi\sec^2\left(\frac{\pi}{4}-\frac{\varphi}{2}\right). \tag{A7}$$

The energy dissipation work of *ACO* due to self-weight

$$W_{G_1} = -\frac{1}{6}\gamma\pi R^3 v_\mathrm{p}\tan\left(\frac{\pi}{4}-\frac{\varphi}{2}\right). \tag{A8}$$

Logarithmic spiral zone *AFC*

Incremental internal work due to Logarithmic spiral *FCHG*

$$W_2=\int_0^{\frac{\pi}{2}}2\pi vc\cos\varphi\left[\frac{R}{2}-r\cos\left(\frac{\pi}{4}-\frac{\varphi}{2}+\theta\right)\right]\frac{r}{\cos\varphi}\mathrm{d}\theta=\frac{1}{2}v_{\mathrm{p}}c\pi R^2\sec^2\left(\frac{\pi}{4}-\frac{\varphi}{2}\right)\left[\frac{1-\mathrm{e}^{-\pi\tan\varphi}}{2\tan\varphi}-f_1+\tan\left(\frac{\pi}{4}-\frac{\varphi}{2}\right)f_2\right],\tag{A9}$$

where f_1 and f_2 are reported in Appendix B.

Incremental internal work due to the Logarithmic spiral deformation *AFC*

$$W_4=\int_0^{\frac{\pi}{2}}\int_0^{r}2\pi cv\cos\varphi\left[\frac{R}{2}-\bar{r}\cos\left(\frac{\pi}{4}-\frac{\varphi}{2}+\theta\right)\right]\frac{\mathrm{d}\bar{r}}{\cos\varphi}\mathrm{d}\theta=\frac{1}{2}v_{\mathrm{p}}c\pi R^2\sec^2\left(\frac{\pi}{4}-\frac{\varphi}{2}\right)\left[\frac{1-\mathrm{e}^{-\pi\tan\varphi}}{2\tan\varphi}-\frac{1}{2}f_1+\frac{1}{2}\tan\left(\frac{\pi}{4}-\frac{\varphi}{2}\right)f_2\right].\tag{A10}$$

The energy dissipation work of *AFC* due to self-weight

$$W_{G_2}=-\gamma\int_0^{\frac{\pi}{2}}\int_0^{r}2\pi v_v\left[\frac{R}{2}-\bar{r}\cos\left(\frac{\pi}{4}-\frac{\varphi}{2}+\theta\right)\right]\bar{r}\mathrm{d}\bar{r}d\theta=\frac{1}{8}\gamma v_{\mathrm{p}}\pi R^3\sec^2\left(\frac{\pi}{4}-\frac{\varphi}{2}\right)\left\{-f_1+\tan\left(\frac{\pi}{4}-\frac{\varphi}{2}\right)f_2+\frac{1}{3}\sec^2\left(\frac{\pi}{4}-\frac{\varphi}{2}\right)\left[\frac{1-\mathrm{e}^{-2\pi\tan\varphi}}{4\tan\varphi}+\cos 2\left(\frac{\pi}{4}-\frac{\varphi}{2}\right)f_3-\sin 2\left(\frac{\pi}{4}-\frac{\varphi}{2}\right)f_4\right]\right\},\tag{A11}$$

where f_3 and f_4 are reported in Appendix B.

3. Wedge zone *AEF*

Incremental internal work due to the wedge *AEF*

$$W_3=(v_1\cos\varphi)cS_{\overline{EFGD}}=\frac{1}{4}v_{\mathrm{p}}c\pi R^2\cos\varphi\sec^2\left(\frac{\pi}{4}-\frac{\varphi}{2}\right)\mathrm{e}^{-\pi\tan\varphi}\left[3\tan\left(\frac{\pi}{4}-\frac{\varphi}{2}\right)\mathrm{e}^{-\frac{\pi}{2}\tan\varphi}+2\right]\tag{A12}$$

The energy dissipation work of *AEF* due to self-weight

$$W_{G_3}=\frac{1}{6}\gamma\pi R^3v_{\mathrm{p}}\tan^2\left(\frac{\pi}{4}-\frac{\varphi}{2}\right)\mathrm{e}^{-\frac{3}{2}\pi\tan\varphi}\left[\tan\left(\frac{\pi}{4}-\frac{\varphi}{2}\right)\mathrm{e}^{-\frac{\pi}{2}\tan\varphi}+2\right]\tag{A13}$$

4. Incremental external work due to the surcharge loading

$$W_q=v_{\mathrm{p}}\pi R^2\tan^2\left(\frac{\pi}{4}-\frac{\varphi}{2}\right)\mathrm{e}^{-\pi\tan\varphi}\left[\tan\left(\frac{\pi}{4}-\frac{\varphi}{2}\right)\mathrm{e}^{-\frac{\pi}{2}\tan\varphi}+2\right]q\tag{A14}$$

5. Energy dissipation work on the interface of the caisson outer wall and the soil

$$W_6=2\pi RLacv_{\mathrm{p}}\tag{A15}$$

6. Eenergy dissipation rate of soil gravity in suction caisson

$$W_{G_4}=-\gamma v_{\mathrm{p}}\pi R^2L\tag{A16}$$

7. Incremental external work due to the uplift load

$$W_{F_2}=v_{\mathrm{p}}F_2,\tag{A17}$$

where F_2 is the uplift load.

8. Formulation of upper bound solution

Equating the work rates of external loads to the total internal energy dissipation rates, we can obtain the general equation of the ultimate bearing capacity using upper bound method, which is

$$W_{F_2}+W_q+W_{G_1}+W_{G_2}+W_{G_3}+W_{G_4}=W_1+W_2+W_3+W_4+W_5.\tag{A18}$$

Appendix B

$$f_1=\int_0^{\frac{\pi}{2}}\mathrm{e}^{-3\theta\tan\varphi}\cos\theta\mathrm{d}\theta=\frac{\mathrm{e}^{-\frac{3}{2}\pi\tan\varphi}+3\tan\varphi}{1+(3\tan\varphi)^2};\tag{B1}$$

$$f_2=\int_0^{\frac{\pi}{2}}\mathrm{e}^{-3\theta\tan\varphi}\sin\theta\mathrm{d}\theta=\frac{1-3\tan\varphi\mathrm{e}^{-\frac{3}{2}\pi\tan\varphi}}{1+(3\tan\varphi)^2};\tag{B2}$$

$$f_3=\int_0^{\frac{\pi}{2}}\mathrm{e}^{-4\theta\tan\varphi}\cos 2\theta\mathrm{d}\theta=\tan\varphi\frac{\mathrm{e}^{-2\pi\tan\varphi}+1}{1+(2\tan\varphi)^2};\tag{B3}$$

$$f_4=\int_0^{\frac{\pi}{2}}\mathrm{e}^{-4\theta\tan\varphi}\sin 2\theta\mathrm{d}\theta=\frac{1}{2}\frac{1+\mathrm{e}^{-2\pi\tan\varphi}}{1+(2\tan\varphi)^2};\tag{B4}$$

$$f_5=\pi R^2\sec^2\left(\frac{\pi}{4}-\frac{\varphi}{2}\right);\tag{B5}$$

$$f_6=\pi R^2\tan^2\left(\frac{\pi}{4}-\frac{\varphi}{2}\right);\tag{B6}$$

$$f_7=\tan\left(\frac{\pi}{4}-\frac{\varphi}{2}\right)\mathrm{e}^{-\frac{\pi}{2}\tan\varphi}.\tag{B7}$$